Intrinsic Properties of Pure and Mixed Monolayer Oxides in the Honeycomb Structure: M2O3 and MM'O3 (M, M' = Ti, V, Cr, Fe)

Jacek Goniakowski, Claudine Noguera

Intrinsic Properties of Pure and Mixed Monolayer Oxides in the Honeycomb Structure: M_2O_3 and MM'O_3 (M, M' = Ti, V, Cr, Fe).

J. Goniakowski* and C. Noguera*

CNRS-Sorbonne Université, UMR 7588, INSP, F-75005 Paris, France

E-mail: jacek.goniakowski@insp.jussieu.fr; claudine.noguera@insp.jussieu.fr

*To whom correspondence should be addressed

Abstract

The growing interest of modern technologies in oxide materials and the advances in the fabrication and control of ultra-thin oxide films raise new questions on how to use cation doping or mixing to engineer the properties of such two dimensional objects. With a special focus on their intrinsic properties in the absence of interaction with a substrate, we have modeled a series of free-standing pure M_2O_3 and mixed $MM'O_3$ compounds (M, M' = Ti, V, Cr, Fe) in two-dimensional honeycomb structures within DFT+U and hybrid approaches. A systematic comparison with their bulk counterparts enabled the identification and discussion of their properties which are driven by their low dimensionality and peculiar atomic structure. On the one hand, it concerns the mixing-induced changes of cation oxidation states, which are controlled by the structure-dependent characteristics of their band edges. On the other hand, an overall increase of the energetic tendency for cationic mixing in low dimensions is highlighted. This comparison shows that low dimensionality enables stabilization of ternary oxides of compositions and properties with no bulk equivalents, thus of a direct interest for modern technologies.

1 Introduction

Two-dimensional (2D) materials, such as graphene, silicene, germanene, hexagonal boron nitride, or transition metal dichalcogenides, have been the subject of intense research during the last decade. Aside from promising applications, they have revealed several peculiar physical phenomena resulting from their reduced dimensionality and size, responsible for novel electronic, optical and transport properties.

In parallel to the studies on these 2D van der Waals materials, much progress has been also made in the synthesis and characterization of ultra-thin oxide films and in particular oxide monolayers.[1] Surprisingly, their structure is in most cases different from what could be expected from a rigid cut of the bulk lattice. Indeed, monolayers (MLs) of most rock-

salt or wurtzite oxides display a graphitic-like structure with six-membered rings, as shown for MgO,[2] ZnO,[3,4] BeO,[5] FeO,[6,7] or CoO.[8,9] Other honeycomb-type (HC) structures with twelve-membered rings have been observed in monolayers of sesquioxides crystallizing in the corundum structure, such as Ti_2O_3,[10–13] and V_2O_3.[14,15] The same is true for the copper oxide Cu_3O_2 monolayer synthesized on Au(111).[16] Monolayers of Ti_2O_3, Mn_2O_3, Co_2O_3, and Ni_2O_3 have also been most recently analyzed theoretically.[17]

While perfectly flat when unsupported, the atomic and electronic structures of such oxide monolayers are additionally modified by the interaction and the electron exchange with the substrate.[13,18,19] As a consequence, the characteristics of supported oxide monolayers strongly differ from those of their parent materials, either bulk or thick films.[17,20–24] The most prominent examples include unusual oxidation states of cations,[13,25] altered stability and electronic structure of point and line defects such as vacancies,[26,27] or edges,[28,29] etc.

The properties of oxide materials may be significantly tuned by doping or alloying, since combining two cations of different size, electronegativity and reducibility, gives an additional lever for modifying the oxide structural, electronic, and reactivity characteristics. In particular, this has been demonstrated both experimentally[30–32] and theoretically,[33–37]in strongly doped bulk corundum oxides and in the $FeWO_3$ HC ML supported on Pt(111).[38] In previous studies, relying on first principles simulations, we have considered a series of mixed transition metal oxides MM'O_3 in bulk corundum-like structures[39] and M_2O_3/M'$_2O_3$ interfaces[40] (M, M' = Ti, V, Cr, and Fe). We have highlighted the existence of a mixing-induced change of cation oxidation states in some of them, and have analyzed its reasons and consequences.

The present work considers the same series of mixed MM'O_3 oxides but focuses on their 2D analogs which adopt a monolayer HC structure. In order to first rationalize the intrinsic properties of such 2D oxides, we have restricted the present analysis to unsupported films. Although not stable with respect to their bulk counterparts, they represent well-defined intermediates between corundum bulks and metal-supported honeycombs (observed experimentally), enabling the identification of intrinsic (dimensionality- and atomic-structure-driven)

features, in the absence of substrate-induced effects. The analysis of metal-supported oxide honeycombs will be the subject of the forthcoming study. Here we thus consider unsupported MM'O_3 HC monolayers (50% composition) with two alternative cationic arrangements to assess the effect of cationic mixing on structural, electronic, and energetic characteristics. The computational results enable to establish and discuss the link to the properties of the corresponding pure parent M_2O_3 HC monolayers, and to highlight the differences in cationic mixing in HC monolayers and bulk corundum materials.

The paper is organized as follows. After a section devoted to the computational method and set-up (Sec. 2), we present and discuss the properties of pure M_2O_3 monolayers (Sec. 3). Section 4 reports the results obtained for the mixed oxides, which are then discussed in Sec. 5, before a conclusion.

2 Computational methods

DFT calculations were performed with the Vienna Ab-initio Simulation Package (VASP),[41,42] using the Projector Augmented Wave (PAW) method[43,44] to represent the electron-core interaction, and a 400 eV energy cutoff in the development of Kohn-Sham orbitals on a plane-wave basis set. Transition metal (TM) $3p$ orbitals were systematically considered as semi-core states. A dispersion-corrected (optB88-vdW[45–47]) exchange-correlation functional was employed within the DFT+U approach proposed by Dudarev.[48,49] As in our previous study,[39] we have used U values close to those reported in the literature: 1.0 eV, 1.7 eV, 3.0 eV, and 3.0 eV for Ti_2O_3, V_2O_3, Cr_2O_3, and Fe_2O_3, respectively, which were shown to yield satisfactory bulk electronic structure characteristics including the gap widths. For each cation we have systematically used the same U values in calculations on both pure M_2O_3 and mixed MM'O_3 oxide honeycombs. Moreover, we have performed systematic complementary hybrid (HSE03)[50,51] calculations to test the sensitivity of our results to the choice of the exchange correlation functional (see Supporting Information (SI)). All calculations were spin-polarized

and the relative stability of simple non-magnetic (NM), and alternative parallel (FM) and anti-parallel (AF) spin orders was systematically tested. Ionic charges were estimated with the partition scheme proposed by Bader,[52,53] and magnetic moments were obtained by integration of the spin density within the Bader's volumes. Atomic configurations were plotted with VESTA.[54]

We have considered flat unsupported HC monolayers of M_2O_3 and MM'O_3 compositions (M, M' = Ti, V, Cr, Fe). As shown in Fig. 1a-b, these monolayers may be viewed as (fully relaxed) single MO_3M or MO_3M' tri-layers cut out of the 3D corundum or ilmenite lattices. Contrary to their distorted octahedral bulk environment, the cations in the HC lattice have their coordination number reduced to three. In the mixed layers two configurations were explored (Fig. 1c-d), either with cations alternating in all directions (A-HC), or arranged in rows (R-HC). A (1×1) unit cell with two cations in high symmetry positions was used for pure and mixed A-HC monolayers. The R-HC configurations were represented in a (2×1) unit cell, containing two cations of each type. In this case only the cations of one type were fixed in high symmetry positions. The remaining cations and all anions were allowed to relax until forces became smaller than 0.01 eVÅ^{-1}. The Brillouin zones of the two unit cells were sampled with Γ-centered $(8 \times 8 \times 1)$ and $(4 \times 8 \times 1)$ Monkhorst-Pack grids, respectively.[55]

The formation energies of mixed MM'O_3 oxides (per formula unit) was estimated with respect to their pure honeycomb M_2O_3 and M'$_2O_3$ monolayer parents:

$$\mathrm{E^{form}} = \mathrm{E_{MM'O_3}} - \frac{\mathrm{E_{M_2O_3}} + \mathrm{E_{M'_2O_3}}}{2} \tag{1}$$

in which $\mathrm{E_{M_2O_3}}$, $\mathrm{E_{M'_2O_3}}$ and $\mathrm{E_{MM'O_3}}$ are the total energies of a formula unit of M_2O_3, M'$_2O_3$ and MM'O_3 in the honeycomb structure, respectively.

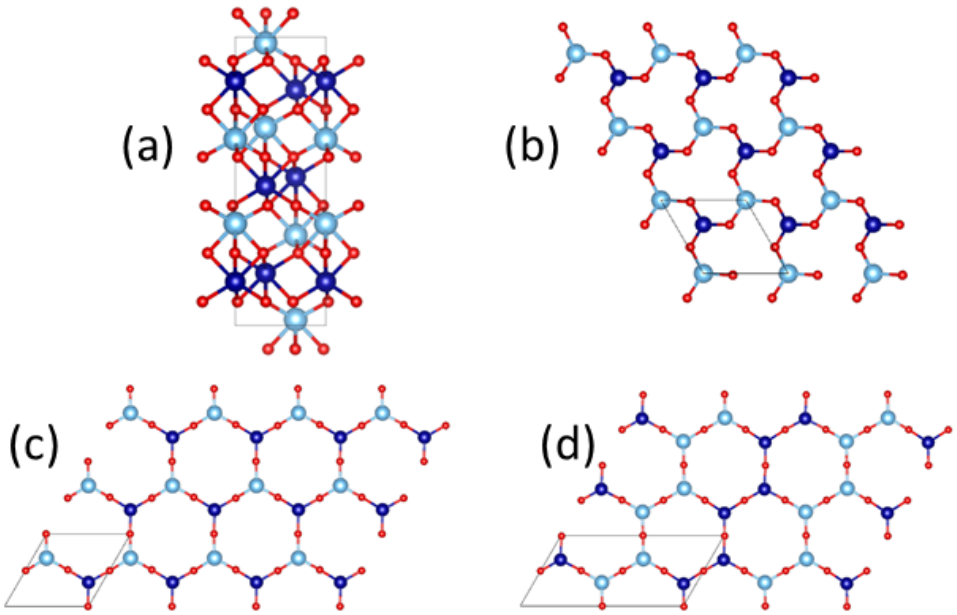

Figure 1: Atomic structures of (a) bulk corundum-like $MM'O_3$ oxide with an ilmenite-type cationic order; (b) mixed $MM'O_3$ monolayer rigidly cut out from the bulk structure; (c) mixed $MM'O_3$ (alternating A-HC configuration) and (d) mixed $MM'O_3$ (row R-HC configuration) fully relaxed monolayers. In each case, the unit cell is indicated. Cations and oxygen atoms are represented by big blue (light and dark) and small red balls, respectively.

3 Results on pure M_2O_3 honeycomb monolayers

This section focuses on pure M_2O_3 HC monolayers (M = Ti, V, Cr, and Fe). We first present the results on their structural and electronic properties. Then we compare them to those obtained for their bulk corundum counterparts.

3.1 Structural and electronic properties

Table 1 summarizes the structural, electronic, magnetic, and energetic characteristics obtained for the pure HC oxides under consideration. Their local densities of states (LDOS) projected on cations and oxygen atoms are displayed in Fig. 2. Corresponding results obtained with the hybrid approach are given in SI, Tab. S1 and Fig. S1.

Table 1: Calculated characteristics of pure M_2O_3 honeycomb oxides (M = Ti, V, Cr, Fe): Lattice parameter a (Å), cation-oxygen bondlengths d_{M-O} (Å), Bader charges (e) on cations Q_M and oxygen atoms Q_O, gap width G (eV), cation magnetic moment μ_M (μ_B), and ground state spin order (MS). FM and AF denote ferromagnetic and antiferromagnetic orders, respectively. Values in parenthesis recall the corresponding results for the M_2O_3 bulk corundum oxides.[39]

	Ti_2O_3	V_2O_3	Cr_2O_3	Fe_2O_3
a	6.37	6.24	6.21	6.20
d_{M-O}	1.84	1.80	1.79	1.79
	(2.03, 2.09)	(1.99, 2.09)	(1.99, 2.05)	(1.95, 2.13)
Q_M	1.74	1.62	1.58	1.63
	(1.91)	(1.84)	(1.76)	(1.74)
Q_O	-1.16	-1.08	-1.06	-1.09
	(-1.27)	(-1.23)	(-1.18)	(-1.16)
G	1.2	0.2	1.4	1.4
	(0.0)	(0.4)	(2.8)	(1.7)
μ_M	0.9	2.1	2.9	3.9
	(0.0)	(1.7)	(2.9)	(4.0)
MS	AF	FM	AF	AF
	(NM)	(G-AF)	(G-AF)	(C-AF)

Due to the similarity of their ionic radii (0.67 Å, 0.64 Å, 0.615 Å and 0.645 Å,[56] for Ti^{3+}, V^{3+}, Cr^{3+}, and Fe^{3+} in its high spin configuration, respectively) the lattice parameters a and the oxygen-cation first neighbor distances d_{M-O} are similar in all M_2O_3 MLs, with only

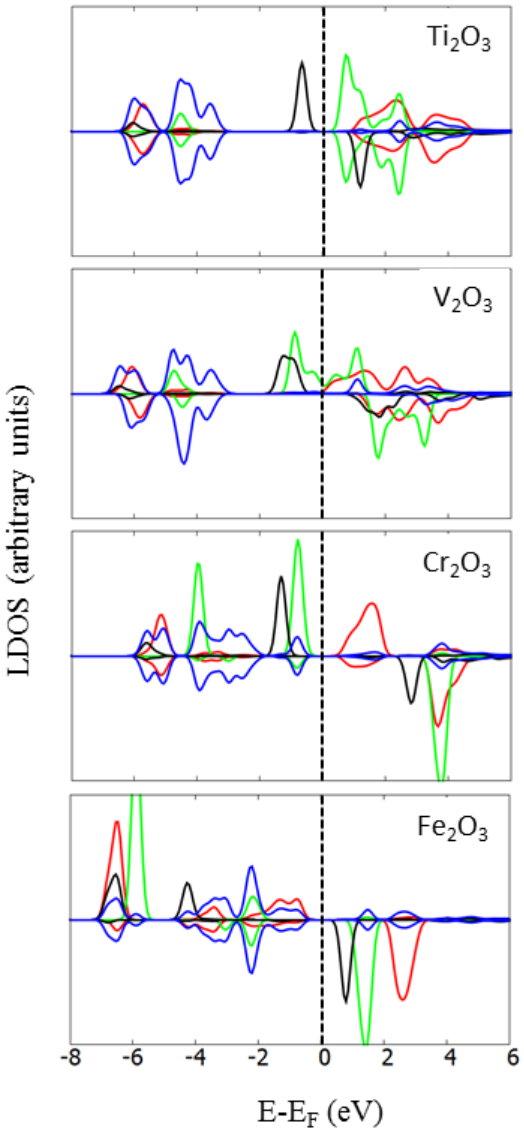

Figure 2: Densities of states in pure M_2O_3 honeycomb monolayers. Black, red and green curves refer to projections on cation d_{z^2}, $\{d_{x^2-y^2}, d_{xy}\}$ and $\{d_{xz}, d_{yz}\}$ orbitals, respectively. The LDOS on oxygen atoms is represented in blue. A broadening of 0.2 eV has been systematically applied. Vertical dashed lines indicate the position of the Fermi level E_F.

a weak systematic decrease along the series.

As far as the electronic structure is concerned, Fig. 2 shows that Ti_2O_3 and V_2O_3 are Mott-Hubbard semi-conductors with purely cationic states at the top of the valence band (VBM) and at the bottom of the conduction band (CBm). While in Ti_2O_3 the filled majority d_{z^2} state is located 1.2 eV below the CBm, the presence of an additional electron in vanadium shifts the V_2O_3 Fermi level into a band of a mixed d_{xz}, d_{yz} and d_{z^2} character, which drastically reduces the gap width. In Cr_2O_3 and Fe_2O_3 the cation states at the VBM are hybridized with oxygen orbitals, thus conferring a mixed charge-transfer and Mott-Hubbard character to these two oxide MLs. In Cr_2O_3 the filled d states just below the Fermi level have a d_{xz}, d_{yz} (state the closest to E_F) and d_{z^2} character, hybridized principally with oxygen $2p_z$ orbitals. Conversely, in Fe_2O_3 in which the majority d band is completely filled, the VBM has Fe d_{xy}, $d_{x^2-y^2}$ and O $2p$ character, while Fe d_{xz} and d_{yz} orbitals are mostly located about 1.5 eV below the Fermi level. The band gaps in these two oxides are very similar ($\approx$ 1.4 eV). As shown in the SI (Tab. S1 and Fig. S1), the HSE03 approach yields qualitatively similar electronic characteristics with nevertheless a larger bond ionicity and much larger gap widths (nearly twice the DFT+U values). A similar trend is also found for the bulk M_2O_3 results, where however the HSE03 gap widths of V_2O_3, Cr_2O_3, and Fe_2O_3 (1.8, 4.0 and 3.2 eV, respectively) are by far too large compared to the corresponding experimental values of 0.0, 3.4, and 2.2 eV. Interestingly, in the case of bulk Ti_2O_3 both DFT+U and HSE03 gaps are very similar and consistent with the experimental evidence. The much larger HSE03 gap obtained for the Ti_2O_3 honeycomb suggests an environment-induced increase of the effective on-site Coulomb interaction, which could be mimicked by an increase of U_{Ti} to about 4 eV.

The cation magnetic moments μ_M increase progressively along the series and follow closely the filling of the $3d$ band (formally 1, 2, 3, and 5 electrons in the high spin configurations of Ti_2O_3, V_2O_3, Cr_2O_3, and Fe_2O_3, respectively). While in the first three oxides, μ_M is nearly equal to the d band filling, in Fe_2O_3, due to a stronger hybridization between iron and oxygen orbitals, μ_M is smaller than 5. In all cases, HSE03 and DFT+U results differ by less than

0.2 μ_B only (SI Tab. S1). The preferential magnetic coupling is anti-ferromagnetic except for V_2O_3 where FM order is favored. The energy difference between the two spin-polarized solution is relatively small in Ti_2O_3 ($\approx$ 0.05 eV per formula unit) and Cr_2O_3 ($\approx$ 0.15 eV) but becomes large ($\approx$ 1 eV) in V_2O_3 and Fe_2O_3.

3.2 Comparison with bulk corundum

Due to the different local environment of ions, M_2O_3 HC monolayers display several characteristics which distinguish them from their corundum-like bulk analogs.[39]

Unsurprisingly, the oxygen-cation bonds in the honeycomb layers are systematically shorter ($\approx$ 0.2 Å) than in the corresponding bulk crystals, Tab. 1, matching the usual trend for a contraction of interatomic distances when the atomic coordination decreases.[57]

More interestingly, the ionic charges vary only weakly along the HC and bulk series (0.10 e and 0.15 e, respectively), with the HC charges being somewhat smaller than the bulk ones (by $\approx$ 0.2 e), Tab. 1. This may suggest that the iono-covalent character of bonds is very similar in all these oxides.

However, such a conclusion does not take into account the increasing number of filled anti-bonding cation-oxygen states in the series. Indeed, within the bond electron transfer model,[58] in simple charge transfer oxides in which only oxygen-cation bonding states are filled, the bond covalency is represented by an electron transfer Δ, which reduces the purely ionic charge of oxygen ($Q_O = -2$) proportionally to the number Z of its first neighbors: $Q_O = -2 + Z\Delta$. However, in transition metal oxides, m cation-oxygen antibonding (AB) states are also filled, inducing an electron back transfer δ per bond and per filled AB state: $Q_O = -2+Z(\Delta-m\delta)$. Within this picture, a nearly constant oxygen charge in the transition metal oxide series of a given structure ($Z = 2$ in HC and $Z = 4$ in the bulk) results from a compensation between increases of both Δ and m. This shows that the bond covalency Δ increases from Ti_2O_3 to Fe_2O_3 in both the bulk corundum and in HC layers, consistent with the progressive lowering of the transition metal d states along the series.[59] Within the same

framework, the systematically smaller Q_O in HC layers than in bulk compounds (smaller Z, same m) leads to the conclusion that bond covalency is larger in the HC. This is to be linked with the reduced separation between cation and oxygen electronic levels and reduced cation-oxygen bond length.[57]

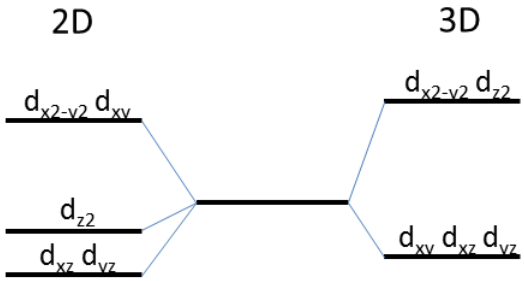

Figure 3: Schematic crystal field splitting of the d levels in (left) a planar trigonal structure and (right) an octahedral environment.

Although the Mott-Hubbard and/or charge-transfer character of the oxides is essentially preserved upon the dimensionality reduction,[39] there are some significant modifications of the electronic structure in the direct vicinity of the Fermi level due to the reduced cation coordination number and the different crystal field splitting of the d orbital manifold. While in the bulk, the quasi-octahedral environment of the cations splits the d orbitals into e_g and t_{2g} multiplets, in the 2D HC geometry the lifting of degeneracy yields three sets involving $\{d_{x^2-y^2}, d_{xy}\}$, $\{d_{xz}, d_{yz}\}$ and d_{z^2} orbitals (Fig. 3). The effect is particularly pronounced in the case of the two Mott-Hubbard insulators (Ti_2O_3 and V_2O_3) for which the directional character of the d orbitals drives substantial changes of VBM and CBm positions when passing from 3D to 2D. The case of Ti_2O_3 provides a paramount example. In corundum bulk it displays a small gap ($\approx$ 0.1 eV) due to a down-shift of a bonding Ti-Ti state from the e_g multiplet, induced by the formation of Ti-Ti pairs along the c crystallographic axis.[39] Conversely, in the HC structure, where such Ti-Ti bonds are absent and the crystal field splitting is different, the highest occupied orbital displays a quasi-atomic d_{z^2} character and is separated from the remaining unoccupied d states by as much as 1.2 eV. As a consequence, while the Ti magnetic moment is quenched in the bulk, it recovers its $\approx 1\ \mu_B$ value, consistent

with the presence of a single electron in the majority d_{z^2} state. Differences in the electronic structure are also noticeable in V_2O_3. In the bulk, its ground state is semi-conducting with a small (≈ 0.4 eV) gap, whereas different crystal field splitting and metal-oxygen hybridization in the HC structure reduce the band gap down to ≈ 0.2 eV.

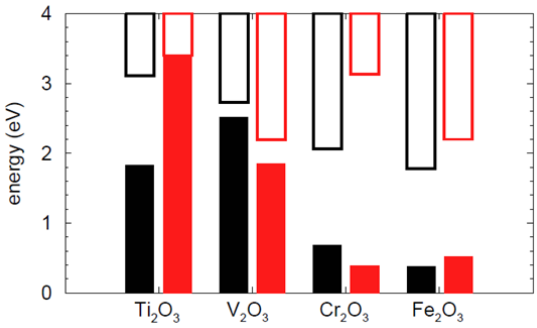

Figure 4: Relative positions of the valence and conduction band edges of the four oxides under consideration, as obtained by alignment of their oxygen $1s$ levels, in the HC (black) and bulk corundum (red) structures.

Figure 4 summarizes the relative positions of the band edges in the four oxides under consideration in both the HC MLs and the bulk corundum, after alignment of their oxygen $1s$ levels. The position of these latter has been systematically estimated from the electrostatic potential at the ionic cores, but test calculations performed in selected cases showed a very good agreement (to within 0.1 eV) with values obtained from a more complete estimation within the PAW approximation. Unsurprisingly, the band edge positions turn out to be more sensitive to the cation environment in the Mott-Hubbard oxides (Ti_2O_3 and V_2O_3) than in Cr_2O_3 and Fe_2O_3. The most pronounced difference concerns Ti_2O_3 for which the VBM is lower (by ≈ 1.4 eV) in the HC ML than in the bulk. Similarly, the change of the band edges in V_2O_3 is due to the 0.4 eV upward shift of the top of its valence band and to the gap decrease when moving from the bulk crystal to the HC layer. Conversely, Cr_2O_3 and Fe_2O_3 display similar VBM in the bulk and HC structures but the Cr_2O_3 CBm is noticeably lowered in the honeycomb structure due to a gap reduction. It is worth noticing that, despite systematically larger band gaps obtained in hybrid calculations, the relative positions of the band edges in the series of the four considered oxides and the changes between bulk corundum

and HC structures are very similar within the DFT+U and HSE03 approaches (SI Fig. S2).

In summary, we have shown that the reduction of lattice dimensionality and the resulting change of the atomic structure have several consequences on the oxide properties. Beyond a systematic shortening of metal-oxygen bonds accompanied by a decrease of their ionic character, we find that the electronic structure of Mott-Hubbard semi-conductors is profoundly modified by the changes of crystal field splitting and orbital hybridization. In the following, we will show that these modifications have a non-negligible impact on the electronic characteristics of the mixed 2D compounds.

4 Results on mixed MM'O_3 honeycomb oxides

This section starts by providing a comprehensive description of the mixed MM'O_3 compounds (M, M' = Ti, V, Cr, and Fe) in their A-HC structure, which is the most stable for most of them. Further on, the dissimilarities between the two alternative A-HC and R-HC structures are highlighted.

4.1 Alternating A-HC structure

Relying on the calculated structural, electronic, magnetic, and energetic characteristics of the mixed MM'O_3 oxides in the A-HC structure, Tab. 2, Figs. 5 and 6 (SI, Tab. S2, Figs. S3 and S4, respectively for the corresponding hybrid results), it appears that the six compounds may be split into two groups, depending on how much their properties differ from those of their parent M_2O_3 and M'$_2O_3$ HC layers. Indeed, while in $TiVO_3$, $TiCrO_3$ and $CrFeO_3$ the mixing induces minor modifications, $TiFeO_3$, $VCrO_3$ and $VFeO_3$ display substantial changes of their properties, which can be assigned to a total or partial change of the cation oxidation states.

From a structural point of view, mixed oxides experience small elastic distortions with respect to their parents. Most of their M-O first neighbor distances d_{M-O} are little mod-

Table 2: Characteristics of mixed MM'O_3 honeycomb oxides (M, M' = Ti, V, Cr, Fe) in the alternating A-HC structure: lattice parameter a (Å), first neighbor distances d_{M-O} and $d_{M'-O}$ (Å), Bader charges (e) on cations Q_M, $Q_{M'}$ and oxygen atoms Q_O, gap widths G (eV), magnetic moments μ_M, $\mu_{M'}$ on cations and total magnetic moment per formula unit μ_{tot} (μ_B), magnetic structure MS, and formation energy E^{form} with respect to the pure honeycomb parents (eV per formula unit). FM and AF denote parallel and anti-parallel spin orders.

	$TiVO_3$	$TiCrO_3$	$TiFeO_3$	$VCrO_3$	$VFeO_3$	$CrFeO_3$
a	6.31	6.27	6.30	6.28	6.24	6.25
d_{M-O}	1.82	1.82	1.77	1.75	1.73	1.78
$d_{M'-O}$	1.82	1.82	1.88	1.88	1.88	1.83
Q_M	1.80	1.82	2.09	1.83	1.88	1.71
$Q_{M'}$	1.59	1.57	1.33	1.45	1.35	1.52
Q_O	-1.13	-1.13	-1.14	-1.09	-1.08	-1.08
G	0.0	0.2	1.2	0.0	1.7	1.2
μ_M	0.8	0.9	0.1	1.5	1.3	2.7
$\mu_{M'}$	2.2	3.2	3.6	3.6	3.6	4.0
μ_{tot}	3	4	4	5	5	2
MS	FM	FM	FM	FM	FM	AF
E^{form}	0.30	-0.23	-0.70	-0.21	-0.79	-0.21
Conf.	$Ti^{3+}V^{3+}$	$Ti^{3+}Cr^{3+}$	$Ti^{4+}Fe^{2+}$	$V^{(4-\delta)+}Cr^{(2+\delta)+}$	$V^{4+}Fe^{2+}$	$Cr^{3+}Fe^{3+}$

ified (less than 0.02 Å). However, in $TiFeO_3$, $VCrO_3$ and $VFeO_3$, d_{M-O} (M = Ti, V) are substantially enhanced and $d_{M'-O}$ (M' = Fe, Cr) are substantially reduced ($\approx$ 0.07-0.09 Å) with respect to the parent structures. Such changes suggest a mixing-induced increase of the oxidation state of M and a decrease in M'. Indeed, the ionic radii are known to decrease in cations of higher oxidation states, as can be expected from the more attractive cationic charges ($r_{M^{4+}} < r_{M^{3+}} < r_{M^{2+}}$).[56]

The values of the cationic charges Q_M and $Q_{M'}$ follow a similar pattern. Those in $TiFeO_3$, $VCrO_3$ and $VFeO_3$ display pronounced modifications with respect to the parent oxides, while in the remaining three compounds changes are much smaller. Although the Bader charges do not straightforwardly give information on formal charges, the fact that Q_M (M = Ti, V) systematically increased and $Q_{M'}$ (M' = Fe, Cr) systematically decreased (by 0.11-0.34 e) is consistent with the proposed changes of oxidation states. Moreover, also the behavior of the cation magnetic moments μ_M and $\mu_{M'}$ and total magnetic moment μ_{tot} strongly supports

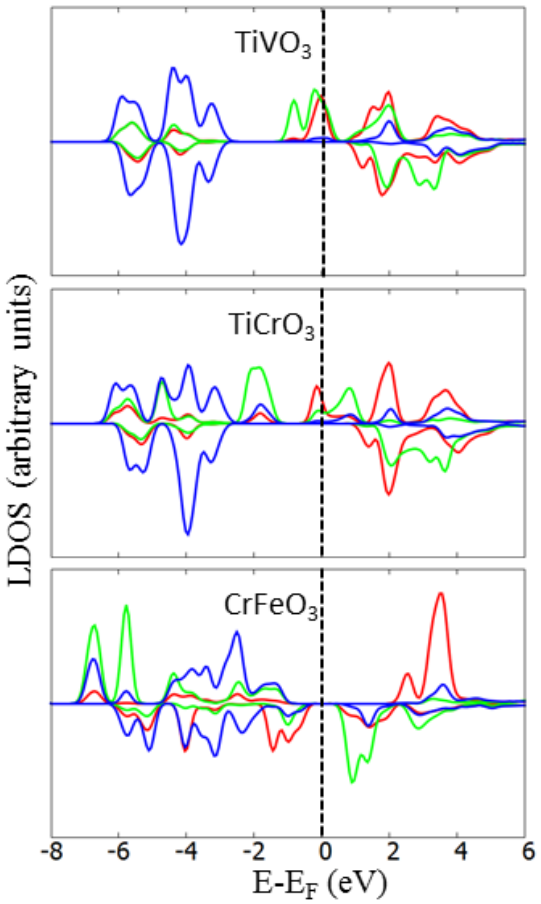

Figure 5: DFT+U densities of states in mixed MM'O_3 honeycomb A-HC structure ($TiVO_3$, $TiCrO_3$ and $CrFeO_3$), projected on M (red) M' (green), and O atoms (blue). A broadening of 0.2 eV has been systematically applied. Vertical dashed lines indicate the position of the Fermi level.

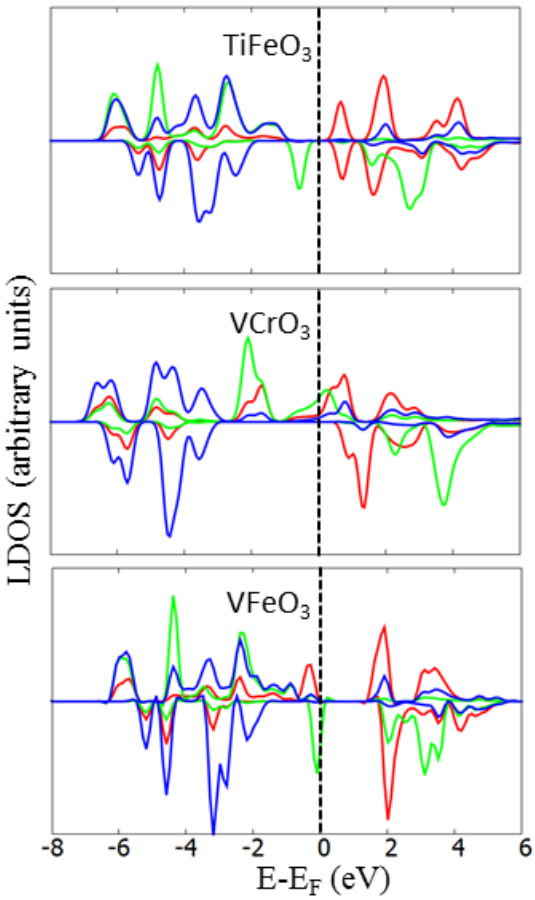

Figure 6: Same as Figure 5 for $TiFeO_3$, $VCrO_3$ and $VFeO_3$.

this picture. Ti bears a nearly vanishing magnetic moment in $TiFeO_3$, characteristic of the loss of its single d electron and leading to a +4 oxidation state. In this compound μ_{tot} is equal to 4 μ_B, while it would be equal to 6 μ_B if no change of oxidation state had occurred. Similarly, in $VFeO_3$, μ_V is smaller by nearly 1 μ_B than in the V_2O_3 parent, consistent with the formal +4 state of vanadium. Again μ_{tot} is equal to 5 μ_B while it would be equal to 7 μ_B if no change of oxidation state had occurred. The case of $VCrO_3$ is slightly less clear and suggests that only a partial redistribution of one electron between the cations takes place. In this case $\mu_{tot} = 5\mu_B$ is the same whatever the strength of the electron exchange between cations. Tab. 2 indicates that parallel spin order is systematically favored, but in $CrFeO_3$.

Finally, the non-negligible changes of Q_M and μ_M are consistent with the LDOS modifications. Clearly, the electronic structures in the vicinity of the Fermi level in $TiFeO_3$, $VCrO_3$, and $VFeO_3$, Fig. 6, differ substantially from those of their parent oxides, Fig. 2, contrary to the remaining three compounds, Fig. 5, where they are essentially a superposition of those of their parents. Indeed, the filled majority Ti peak just below Fermi level, characteristic of the Ti^{+3} oxidation state in Ti_2O_3, is also present in $TiVO_3$ and $TiCrO_3$, although partially intersected by the Fermi level in the former. Conversely, it is shifted above E_F and entirely emptied in $TiFeO_3$. In this latter case, the Fe d_{z^2} orbital, which is located above the Fermi level in Fe_2O_3, is shifted below E_F and populated. Analogous considerations also apply to $VFeO_3$ in which a vanadium peak located below the Fermi level in the parent V_2O_3 HC layer is shifted above E_F and depopulated upon mixing with Fe_2O_3. Due to the localized character of the d levels close to the Fermi level in these Mott-Hubbard compounds and the presence of a non-vanishing gap, a correlated shifts of a whole d state across the Fermi level on dissimilar M and M' cations may take place leading to an actual oxydo-reduction process $M^{3+} + M'^{3+} \longrightarrow M^{4+} + M'^{2+}$ (M = Ti, V; M' = Fe). It is thus legitimate to talk of a change of the cation oxidation states. At variance, due to the metallic character in the LDOS of $VCrO_3$, the redistribution of one electron between the two cations is only partial. We have schematized this configuration in Tab. 2 by $V^{(4-\delta)+}Cr^{(2+\delta)+}$. We note that the

hybrid approach yields fully consistent results (SI, Tab. S2 and Figs. S2 and S3).

Regarding their stability with respect to their HC parents, most mixed HC oxides have negative formation energies E^{form}, thus showing a relatively clear preference for cationic mixing. This preference is particularly well pronounced in $TiFeO_3$ and $VFeO_3$ where the mixing is accompanied by a change of the cation oxidation states. Associated to weaker changes in the electronic structure, the tendency for mixing is weaker in $VCrO_3$. Its E^{form} is smaller and similar to those of $TiCrO_3$ and $CrFeO_3$, which show only small mixing-induced electronic rearrangements. The unique case of a positive formation energy is found in $TiVO_3$. It tells that Ti_2O_3 and V_2O_3 have no tendency to form a mixed A-HC structure at 0K. These energetic characteristics are confirmed in HSE03 calculations. The only discrepancy concerns $VCrO_3$ which, in HSE03, is found to be (weakly) unstable with respect to its HC parents..

To summarize, structural, electronic and magnetic characteristics give a consistent evidence of a total or partial mixing-induced change of cation oxidation states in $TiFeO_3$, $VCrO_3$, and $VFeO_3$, while the electronic characteristics of the remaining three compounds correspond essentially to a superposition of those of their parent oxides. Interestingly, most 2D compounds display non-negligible negative formation energies with respect to their HC parents (tendency for mixing). This characteristic is not systematically correlated to the presence or absence of a mixing-induced redox process, although the largest negative formation energies are found when a full redox process takes place ($TiFeO_3$ and $VFeO_3$).

4.2 Row R-HC structure

As shown in Tab. 3, the characteristics of the mixed MM'O_3 oxides in the R-HC structure differ relatively little from those obtained for the A-HC one, Tab. 2.

This similarity is particularly obvious for the three compounds in which no change of cation oxidation states takes place ($TiVO_3$, $TiCrO_3$, and $CrFeO_3$). Indeed, as in the A-HC structure, both cation charges and magnetic moments in these oxides are nearly equal to those in their parent HC layers, which is consistent with a preservation of the cation +3

Table 3: Same as Table 2 for the row R-HC structure. The three spin orders refer to MM, M'M' and MM' couplings, respectively. O and O' represent oxygen atoms in between cations of different or same type, respectively.

	$TiVO_3$	$TiCrO_3$	$TiFeO_3$	$VCrO_3$	$VFeO_3$	$CrFeO_3$
a	6.31	6.29	6.30	6.29	6.18	6.20
$< d_{M-O} >$	1.84	1.83	1.78, 1.75	1.74	1.69, 1.72	1.75
$< d_{M-O'} >$	1.83	1.85	1.83	1.83	1.77, 1.86	1.81
$< d_{M'-O} >$	1.80	1.81	1.89, 1.91	1.88	1.92, 1.95	1.81
$< d_{M'-O'} >$	1.84, 1.77	1.81	1.80	1.81	1.76, 1.82	1.78
Q_M	1.74	1.75	1.82, 1.93	1.70	1.84, 1.71	1.67
$Q_{M'}$	1.67	1.62	1.56, 1.40	1.55	1.29, 1.59	1.56
$< Q_O >$	-1.14	-1.12	-1.12	-1.08	-1.07	-1.08
G	0.9	0.3	0.0	0.0	0.7	1.3
μ_M	0.9	0.9	0.7, 0.4	1.9	0.9, 1.9	2.8
$\mu_{M'}$	2.0	3.0	4.0, 3.7	3.3	3.4, 4.0	3.9
μ_{tot}	1	0	0.2	5	1	0.1
MS	FM, FM, AF	AF, AF, FM	AF, AF, AF	FM, FM, FM	AF, AF, FM	AF, AF, AF
E^{form}	0.07	-0.07	-0.09	-0.06	-0.14	-0.11
Conf	$Ti^{3+}V^{3+}$	$Ti^{3+}Cr^{3+}$	$Ti^{3+}Fe^{3+}$ $Ti^{(4-\delta)+}Fe^{(2+\delta)+}$	$V^{3+}Cr^{3+}$	$V^{3+,4+}Fe^{2+,3+}$	$Cr^{3+}Fe^{3+}$

oxidation state. Moreover, their lattice parameters a and bondlengths d_{M-O} and $d_{M'-O}$ are systematically close to those in the A-HC structure, despite a dimerization which takes place in $TiVO_3$ along the vanadium rows, with successive d_{V-O} equal to 1.84 and 1.77 Å. Reminiscent of that observed in bulk VO_2 below the Mott-Hubbard-Peierls transition, such dimerization is not possible in the high symmetry A-HC structure. Its presence lowers significantly the formation energy of the R-HC mixed layer with respect to that of A-HC structure.

At variance with these three compounds, $TiFeO_3$, $VFeO_3$ and to some extent $VCrO_3$ display stronger modifications of their atomic and electronic structures, which are essentially in-line with those in the A-HC structure. However, their electronic structure shows several features which are specific to the lower symmetry of the R-HC arrangement and to the resulting possibility of a non-equivalence of the two cations of each type. $VFeO_3$ constitutes a paramount example with charges and especially magnetic moments of the two cations of the same type which significantly differ from each other. One vanadium cation preserves its parent-like magnetic moment $\mu_M \approx 2\ \mu_B$, while the other one is visibly reduced ($\mu_M \approx 1\ \mu_B$). Similar non-uniform changes also concern the magnetic moments $\mu_{M'}$ of the two Fe

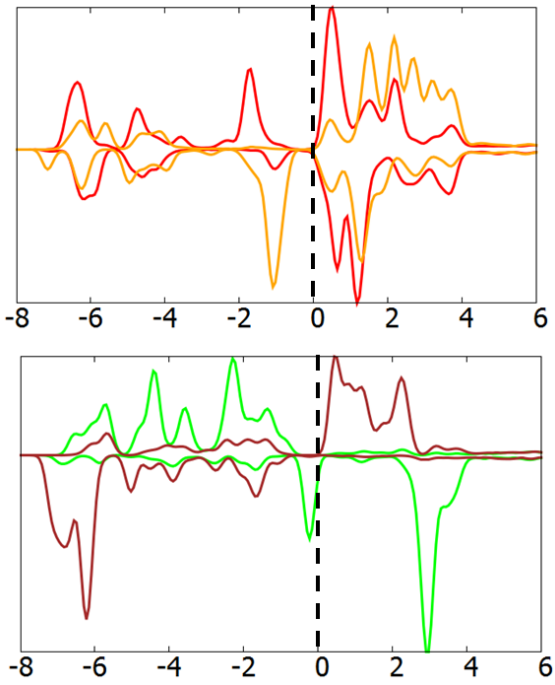

Figure 7: DFT+U LDOS of $VFeO_3$ in R-HC structure projected on the two inequivalent V (top) and Fe (bottom) cations. A broadening of 0.2 eV has been systematically applied. Vertical dashed lines indicate the position of the Fermi level.

cations, one of which is parent-like ($\mu_{M'} \approx 4\ \mu_B$) and the other is reduced ($\mu_{M'} \approx 3.4\ \mu_B$). Such modifications suggest a coexistence of V cations in both 4+ and 3+ oxidation states with Fe^{+2} and Fe^{+3} ions. The local density of states, Fig. 7, fully supports this picture. An unoccupied state localized on one of the two Fe cations is clearly shifted below the Fermi level leading to a formal Fe^{2+} state, while this is not the case for the other Fe cation which preserves its Fe^{3+} configuration. Concomitantly, the single electron (per unit cell) necessary for this transformation in $VFeO_3$ is provided by only one of the two V ions, as shown in Fig. 7 in the vanadium LDOS.

The two cations of similar types in $TiFeO_3$ also bear different charges and magnetic moments. While one Fe ion is clearly in a 3+ oxidation state ($\mu = 4\mu_B$), with no filled minority spin state, the LDOS on the second Fe and the two Ti ions are intercepted by the Fermi level, conferring a metallic character to the compound and making the identification of oxidation state less straightforward. We have schematized this configuration in Tab. 3 by

$Ti^{3+,(4-\delta)+}Fe^{3+,(2+\delta)+}$. In the case of $VCrO_3$, the two V and Cr cations remain equivalent, their charges and magnetic moments are close to those expected for a 3+ oxidation state of each cation, but one is likely at the border line of an electron exchange process since the gap is vanishing.

Finally, the stability of mixed oxides in the R-HC structure, Tab. 3, also follows closely the trends found for the A-HC case, Tab. 2. However, while formation energies remain in most cases negative, their absolute values are systematically reduced compared to the A-HC structure, revealing the lower stability of the R-HC arrangement. This reduction is particularly striking in the case of $TiFeO_3$ and $VFeO_3$ where it is likely linked to the partial only redox process, which concerns a single cation of each type. $TiVO_3$ is the only mixed compound characterized by a positive formation energy. Moreover, at variance with all other compounds, its R-HC configuration is more stable than the A-HC one. The reduction of E^{form} with respect to the A-HC structure is in this case due to a dimerization of V-O bonds enabled by the lower symmetry of the row-wise arrangement. This suggests that a further symmetry breaking could additionally stabilize the 2D $TiVO_3$ oxide.

In summary, while we find that the characteristics of mixed oxides in the R-HC structure are essentially in-line with those obtained for the A-HC arrangement, several non-negligible differences exist and are principally due to the lower symmetry of the R-HC structure. On the one hand, the latter makes possible the electron exchange of a single electron per two cation pairs, resulting in a coexistence of cations of the same type with different oxidation states ($TiFeO_3$ and $VFeO_3$). The tendency for mixing (negative E^{form}) is preserved in R-HC honeycombs, but these structures are systematically less stable than the A-HC ones. On the other hand, row-wise arrangement enables a structural bond dimerization in $TiVO_3$, which considerably stabilizes the R-HC structure with respect to the A-HC one. Despite this stabilizing effect, $TiVO_3$ remains the unique case in which cationic mixing is not favored (positive E^{form}).

5 Discussion

In this last section, we stress the electronic mechanisms which are responsible for the presence or absence of strong modifications of the electronic structure in the mixed HC compounds, with a particular focus on the redox process which takes place in some of them. Further on, we discuss the sensitivity of our results to the choice of the exchange correlation functional. Finally, by comparing the present results with those of our earlier study on the same series of oxides in bulk corundum-like structures,[39] we highlight the different behavior of 2D and 3D mixed compounds and link it to that of the parent oxides.

5.1 Redox processes in mixed MM'O_3 compounds

Our computational results unambiguously show that the characteristics of $TiFeO_3$, $VFeO_3$ and to some extent $VCrO_3$ compounds differ substantially from those of the other mixed oxides, due to the existence of total or partial changes of the cation oxidation states. In order to identify the origin of such redox-type processes and to link them to the electronic characteristics of the parent materials, we have made an analysis of their band alignments. Taking into account that the oxygen lattice is the same in the two parent oxides M_2O_3 and M'_2O_3, we have performed an alignment of their oxygen $1s$ states in the spirit of models used for semiconductor interfaces.[59–67] Once the oxygen $1s$ levels are aligned, the band-offsets between the parent oxides are quantified by two parameters Δ_1 =$E_{CBm}(M'_2O_3)$ - $E_{VBM}(M_2O_3)$ and Δ_2 =$E_{CBm}(M_2O_3)$ - $E_{VBM}(M'_2O_3)$, Fig. 8 (left), related to the difference in VBM positions Δ_{VBM} = $E_{VBM}(M_2O_3)$ - $E_{VBM}(M'_2O_3)$ and to the gaps widths G and G' of the M_2O_3 and M'_2O_3 materials (Tab. 4):

$$\begin{aligned} \Delta_1 &= -\Delta_{VBM} + G' \\ \Delta_2 &= +\Delta_{VBM} + G \end{aligned} \tag{2}$$

Within this definition, negative values of Δ_1 or Δ_2 indicate an overlap between the VBM of one parent oxide and the CBm of the other one, suggesting that redox reactions $M^{3+} + M'^{3+} \longrightarrow M^{4+} + M'^{2+}$ or $M^{3+} + M'^{3+} \longrightarrow M^{2+} + M'^{4+}$, respectively may take place. Corresponding values of Δ_1 and Δ_2 deduced from results of hybrid calculation are given in SI, Tab, S4. Let us note that an analysis of band offsets may also be based on an alignment of the vacuum levels of the parent materials, Fig. 8 (right). To complement the results, the corresponding values of Δ'_1 and Δ'_2 are given in Tab. 4.

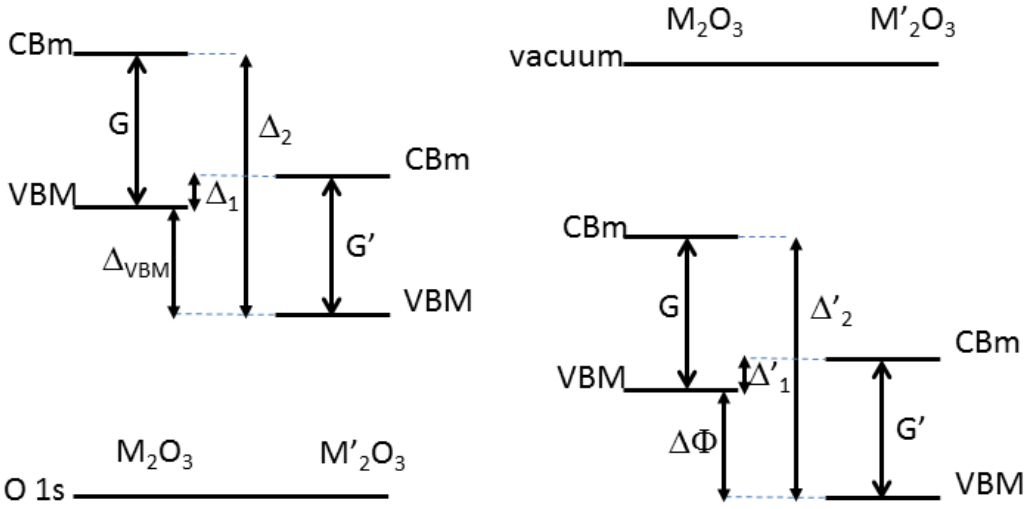

Figure 8: Relative positions of the valence band maximum (VBM) and conduction band minimum (CBm) of the two parent oxides after alignment of (left) their oxygen $1s$ levels or (right) the vacuum level. The meaning of the parameters Δ_1, Δ_2, Δ_{VBM}, Δ'_1, Δ'_2, $\Delta\Phi$, G and G' (see text) is indicated.

We find that Δ_2 values are in all cases positive, Tab. 4, showing that an overlap between the CBm of M_2O_3 and the VBM of M'$_2$O$_3$ never takes place. Thus an M'→M electron transfer is prohibited, which is essentially in agreement with the increase of metal electronegativity in the series Ti, V, Cr, and Fe. Indeed, no such transfers have been found in the full calculation on mixed oxides. Conversely, while Δ_1 is positive for Ti_2O_3-Cr_2O_3, Ti_2O_3-V_2O_3, and Cr_2O_3-Fe_2O_3 (absence of M→M' electron transfer), it becomes negative for V_2O_3-Fe_2O_3 and V_2O_3-Cr_2O_3, thus suggesting a possibility of a significant M→M' electron exchange

Table 4: Values of the parameters Δ_1, Δ_2, and Δ_{VBM} deduced from the band structures of the parent honeycomb oxides M_2O_3 and M'$_2O_3$, after alignment of their oxygen $1s$ levels, Fig. 8(left). G and G' refer to the gaps of M_2O_3 and M'$_2O_3$, respectively. Values of Δ'_1, Δ'_2, and $\Delta\Phi$ refer to the corresponding results obtained by aligning the vacuum levels, Fig. 8(right). The right part of the table recalls the corresponding results obtained for bulk corundum oxides, Ref.[39]

			HC				HC			bulk	
M_2O_3-M'$_2O_3$	Δ_1	Δ_2	Δ_{VBM}	G	G'	Δ'_1	Δ'_2	$\Delta\Phi$	Δ_1	Δ_{VBM}	G'
V_2O_3-Fe_2O_3	-0.7	2.3	2.1	0.2	1.4	-0.1	2.9	1.5	0.4	1.4	1.7
V_2O_3-Cr_2O_3	-0.4	2.0	1.8	0.2	1.4	-0.3	1.9	1.7	1.3	1.5	2.8
Ti_2O_3-Fe_2O_3	0.0	2.7	1.4	1.2	1.4	0.3	2.5	1.1	-1.1	2.8	1.7
Ti_2O_3-Cr_2O_3	0.3	2.3	1.1	1.2	1.4	0.1	2.7	1.3	-0.1	2.9	2.8
Ti_2O_3-V_2O_3	0.9	0.6	-0.7	1.2	0.2	0.6	0.9	-0.4	-1.1	1.5	0.4
Cr_2O_3-Fe_2O_3	1.1	1.7	0.3	1.4	1.4	1.6	1.2	-0.2	1.6	-0.1	1.7

in these two cases. These predictions clearly match the results of the full calculations on the corresponding mixed compounds, even-though the case of Ti_2O_3-Fe_2O_3 in which a redox process takes place is at the border line, with $\Delta_1 = 0$. We note that a similar picture is given by Δ'_1 and Δ'_2, obtained by aligning the vacuum levels of parent oxides. Most interestingly, while systematically shifted towards somewhat more positive values, Δ_1 and Δ_2 obtained within the hybrid approach in both HC and bulk cases (SI, Table S4) do support the above analysis. Indeed, all Δ_2 are positive whereas negative or small positive values of Δ_1 are indicative for cases in which the redox reaction takes place. The only clear exception is the case of HC Ti_2O_3-Fe_2O_3 for which $\Delta_1 = 1.4$ eV is not consistent with a well defined redox reaction in HC $TiFeO_3$ predicted by the full hybrid calculation. This exception highlights the indicative only character of the $\Delta_1 < 0$ criterion. Indeed, the band offsets of the two parent oxides only define the starting configurations for an electron redistribution, while subsequent substantial changes of level positions may take place in response to the electron transfers.

The positive values of Δ_2 are to be ascribed to Δ_{VBM} being larger than zero for all pairs of parent materials except Ti_2O_3-V_2O_3, Fig. 4. However, in this latter case, the negative value of Δ_{VBM} is small enough to be compensated by the large gap G of Ti_2O_3. Negative

Δ_1 are driven principally by large positive $\Delta_{VBM} > G'$. Cases of positive Δ_1 correspond to smaller values Δ_{VBM} and/or larger gaps of the parent M'$_2$O$_3$ material, such that $\Delta_{VBM} < G'$.

Since the gaps of Cr_2O_3 and Fe_2O_3 are nearly equal, the behavior of Δ_1 for the M_2O_3-Cr_2O_3 and M_2O_3-Fe_2O_3 directly reflects that of Δ_{VBM}. At variance, VBM in HC Ti_2O_3 and V_2O_3 are more than 1 eV higher than those of HC Cr_2O_3 or Fe_2O_3 (Fig. 4, Section 3.2). This difference is at the origin of the mixing-induced changes of oxidation states between cations of these two groups. Conversely, since the VBM in Ti_2O_3 and V_2O_3 are close to each other and those in Cr_2O_3 and Fe_2O_3 are practically identical, no pronounced electronic effects occur in $TiVO_3$ or in $CrFeO_3$.

Finally, one can note that, in the cases where no change of oxidation states takes place ($\Delta_1 > 0$), the band offsets also provide a good estimate of band gaps in the mixed compound. Indeed, in $TiCrO_3$ and $CrFeO_3$ where the Fermi level falls in between states of a different cationic character, the values of Δ_1 (0.3 and 1.1 eV, respectively, Table 4) match very well the gap widths obtained from the full calculations (0.2 and 1.2 eV, respectively, Table 2).

In summary, we have shown that, in most cases, the principal features of the electronic structure of mixed honeycomb layers may be inferred from the band offsets between their parent oxides. In particular, the existence of mixing-induced changes of the cation oxidation states is to be principally ascribed to significant differences in the positions of the valence band maximum of the parents. It is higher on a common energy scale in early transition metal oxides of Mott-Hubbard character (Ti_2O_3 and V_2O_3) than in those involving metals from the middle of the series (Cr_2O_3 and Fe_2O_3) and characterized by mixed Mott-Hubbard/charge transfer character.

5.2 Sensitivity to the exchange correlation functional

In view of the well-known difficulty in treating the electronic structure of transition metal oxides, in this section we discuss the sensitivity of our results to the choice of the DFT

exchange-correlation functional. We first compare the reported DFT+U results with the data obtained in hybrid calculations (summarized in SI). Further-on we extend the discussion to the sensitivity of DFT+U results to the choice of U.

Despite their rather different treatment of exchange and correlation effects, the reported DFT+U and HSE03 results give a very consistent description of the electronic structure and energetics of both the pure and mixed HCs. More specifically, for the pure HC layers (DFT+U: Tab. 1 and Fig. 2; HSE03: SI Tab.S1 and Fig. S1), despite a slightly stronger bond ionicity and nearly twice larger gaps in HSE03, both approaches provide identical character of the states close to the Fermi level and cation magnetic moments. Moreover, regarding the band alignments (DFT+U: Tab. 4; HSE03: SI Tab. S4), the signs of Δ_2 are consistently always positive and those of Δ_1 are identical in DFT+U and HSE03 to within 0.1 eV. We note however that HSE03 Δ_1 tend to be more positive, in particular in the Ti_2O_3-Fe_2O_3 case ($\Delta_1 = 1.4$ eV and 0.0 eV in HSE03 and DFT+U, respectively). Regarding the mixed HC layers (DFT+U: Tab. 2, Figs. 5 and 6; SI Tab. S2, Fig. S3 and S4), all electronic properties, magnetic moments, and formation energies of $TiCrO_3$, $TiFeO_3$, $VFeO_3$, and $CrFeO_3$ are fully consistent between the two approaches. Small discrepancies concern $TiVO_3$, for which HSE03 predicts a gap opening (likely due to the large gap in the pure HC V_2O_3 parent) and oxidation states slightly departing from +3, and $VCrO_3$, for which HSE03 formation energy is slightly positive (slightly negative in DFT+U).

While such an excellent agreement between the two sets of results additionally validates our findings, one has to remember that HSE03 does not provide a fully definitive answer to the electronic characteristics of Mott-Hubbard insulators. This is clear when considering the discrepancy between experimental and HSE03 gaps in bulk M_2O_3 oxides (1.8, 4.0, and 3.2 eV in V_2O_3, Cr_2O_3, and Fe_2O_3 respectively, to be compared to experimental values of 0.0, 3.4, and 2.2 eV). Moreover, similarly to the Hubbard U in the DFT+U approach, the percentage of Hartree-Fock exchange in HSE03 method remains disputable and may be not transferable between bulk materials and low dimensional HC monolayers.

In this context, as to further test the sensitivity of our DFT+U results to the choice of the U parameters in the exchange-correlation functional, we have systematically studied the electronic and energetic characteristics of selected A-HC mixed compounds as a function of the U values of their cations. As to cover the most qualitatively different situations, we have chosen $TiCrO_3$ and $TiFeO_3$ compounds, Fig. 9, in which an unambiguous assignment of cation oxidation states was obtained ($Ti^{3+}Cr^{3+}$ and $Ti^{4+}Fe^{2+}$, respectively) and $TiVO_3$ and $VCrO_3$ for which a partial electron transfer between cations takes place (at the border line in HSE03 for the former, in both approaches for the latter), Fig. 10. We have monitored the existence of redox processes in the mixed oxides by the variations of the cation magnetic moments $\Delta\mu$ with respect to the pure parent HC oxides. For each MM'O_3 compounds the evolution of $\Delta\mu_M$, $\Delta\mu_{M'}$, and E_{form} is plotted as a function of either U_M or $U_{M'}$ in a large range of values ($1 \leq U \leq 6$ eV).

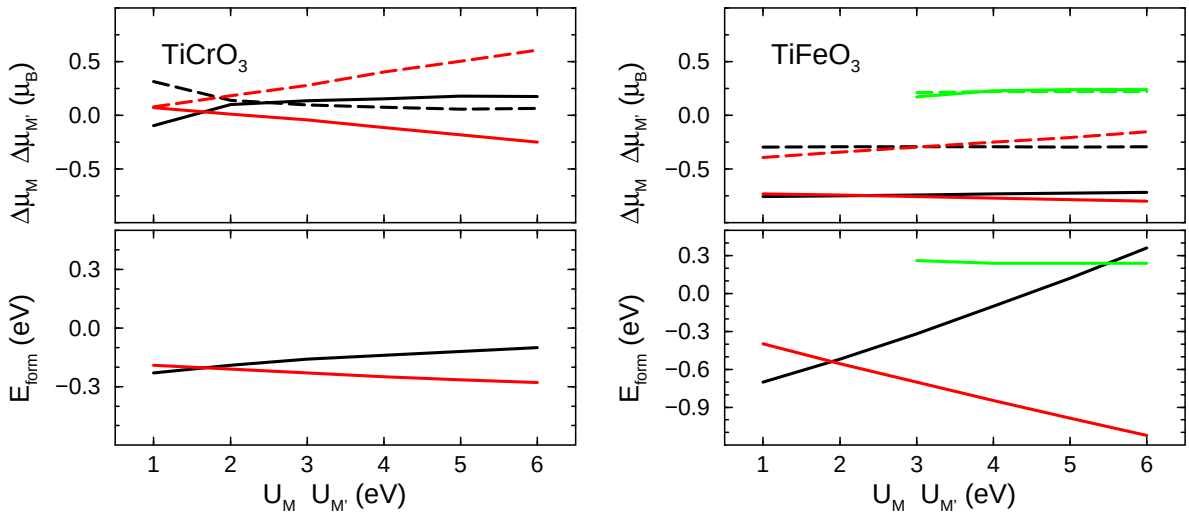

Figure 9: Sensitivity of results for $TiCrO_3$ and $TiFeO_3$ honeycombs to U values: changes of magnetic moments $\Delta\mu_M$ (solid lines) and $\Delta\mu'_M$ (dashed lines) of cations (top) and formation energies E_{form} (bottom) of the mixed MM'O_3 layer with respect to the parent M_2O_3 and M'$_2O_3$ honeycombs. Black and red lines represent behavior as a function of U_M and $U_{M'}$, respectively.

As shown in Fig. 9, the electronic configuration and energetic stability of $TiCrO_3$ and $TiFeO_3$ are essentially insensitive to the variations of U_{Ti}, U_{Cr} or U_{Fe}. Indeed, in $TiCrO_3$,

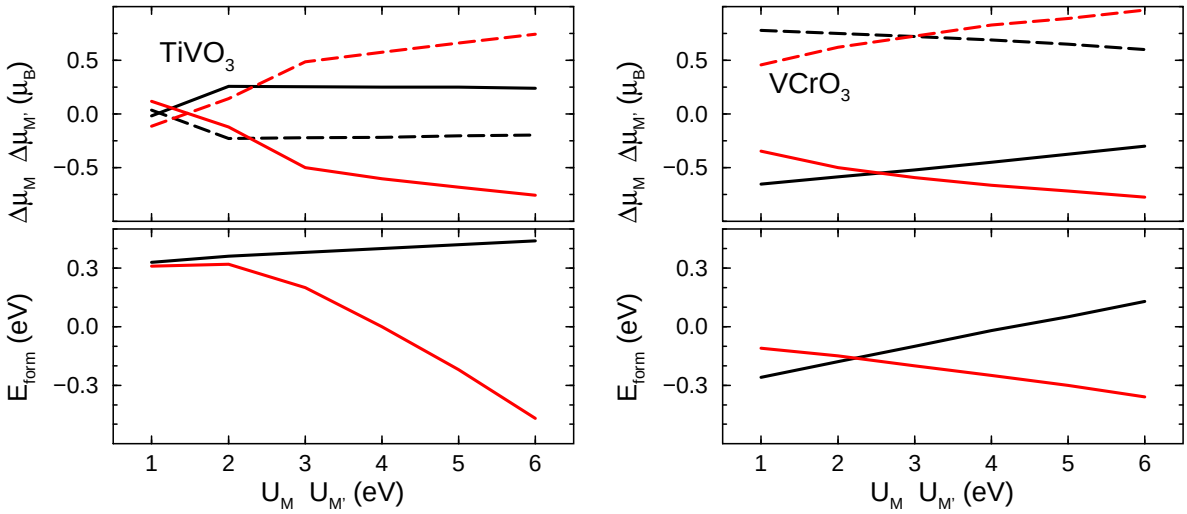

Figure 10: Same as Fig. 9 for $TiVO_3$ and $VCrO_3$ honeycombs.

the cation magnetic moments do not significantly change with U_{Ti} in the whole range of values under consideration. When U_{Cr} is varied, the magnetic moments of both cations depart slightly from their parent values, but huge U_{Cr} values would be required to reach well-defined Ti^{4+} and Cr^{2+} oxidation states. Although the formation energy (weakly) varies with U, $TiCrO_3$ is predicted to be stable with respect to its parents in the whole range of U_{Ti} and U_{Cr} values. In $TiFeO_3$, the magnetic moments of both Ti and Fe remain nearly constant in the whole range of U_{Ti} and U_{Fe} values, at values consistent with Ti^{4+} and Fe^{2+} oxidation states. While E_{form} remains negative when U_{Fe} varies, the structure becomes unstable with respect to the parents at $U_{Ti} \approx 4$ eV. Interestingly, a non-redox state with $E_{form} > 0$ could be obtained in simulations for $U_{Ti} \geq 3$ eV. It becomes favored over the redox state for $U_{Ti} \geq 5$.

For $TiVO_3$ and $VCrO_3$, Fig. 10, a partial electron transfer between cations takes place and is associated with small gap values. In $VCrO_3$ this intermediate state persists in the whole range of considered U values, but with a progressive evolution towards a non-redox state (with $E_{form} > 0$) when U_V increases, or towards a redox state (with $E_{form} < 0$) when U_{Cr} increases. In $TiVO_3$ a progressive transformation towards a well defined redox state starts at $U_V \approx 2$ eV and stabilizes the mixed compound with respect to its parents

($E_{form} < 0$) for $U_V > 4$ eV. Only in this case the results are thus particularly sensitive to the value of U_V and a small increase of U_V brings the DFT+U results very close to the HSE03 predictions.

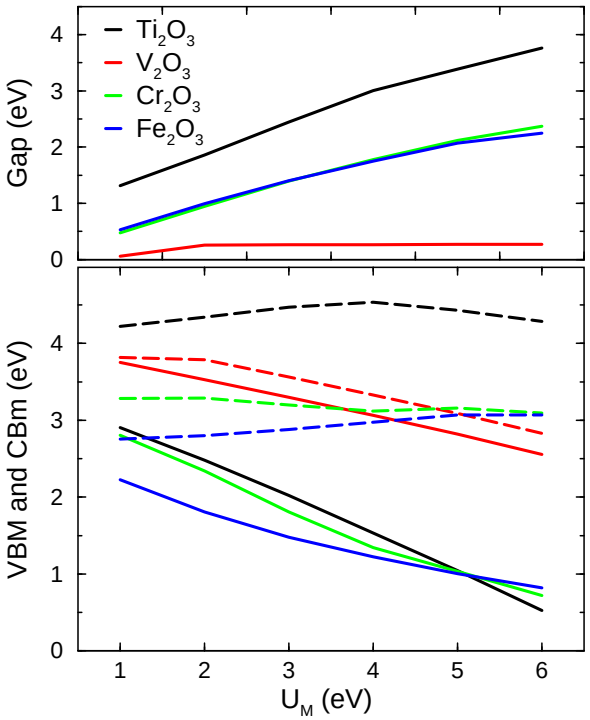

Figure 11: Pure parent M_2O_3 honeycombs: DFT+U values of band gaps (top) and of the relative position of band edges (bottom) as a function of U_M (M = Ti, V, Cr, and Fe). Band structures were aligned by oxygen 1s levels.

A broader view on the sensitivity of redox states to the values of U can be deduced from the variations of band gaps and band-offsets between the pure parents HCs as a function of U, Fig. 11. Unsurprisingly, the increase of U systematically shifts the band structures towards lower energies and simultaneously opens gaps in all oxides but in V_2O_3 HC. As a consequence, all VBM are strongly pushed downwards when U increases, whereas positions of CBm vary much more weakly, except for V_2O_3 where VBM and CBm behave similarly.

These results determine the relatively limited number of cases where crossings between parent VBM and CBm becomes possible. On the one hand, for $U_V > 4$, the VBM of V_2O_3 moves below the CBm of Cr_2O_3 and of Fe_2O_3. On the other hand, for small U_{Ti} and U_{Fe},

the VBM of Ti_2O_3 is to be found below the CMm of Fe_2O_3. Despite their approximate character, these estimations are fairly indicative for the results of the full calculations, where well defined $Ti^{4+}Fe^{2+}$ and $V^{4+}Fe^{2+}$ configurations were found in the mixed $TiFeO_3$ and $VFeO_3$ layers and an onset on a redox reaction has been identified in $VCrO_3$. Moreover, according to Fig. 11, the occurrence of other redox reaction in the considered series can be excluded, regardless the precise U values used in the calculations.

5.3 Comparison with bulk MM'O_3

In a previous study we have analyzed the properties of mixed MM'O_3 oxides (M, M' = Ti, V, Cr, and Fe) in bulk corundum-type structure.[39] In agreement with existing studies,[32–37] we have predicted the existence of mixing-induced redox reactions in bulk $TiVO_3$ and $TiFeO_3$ compounds, resulting in a stabilization of Ti^{4+}, V^{2+}, and Fe^{2+} oxidation states, different from those found in the pure bulk M_2O_3 oxides. The present results show that, despite the same stoichiometry, the changes of cation oxidation states do not concern the same mixed compounds in 2D and 3D. Indeed, redox reactions occur in 3D-$TiVO_3$ but not in its 2D counterpart, the inverse being true for $VFeO_3$ and to some extent for $VCrO_3$. This shows that the cation local environment does considerably impact the electronic characteristics of mixed compounds.

In order to identify the origin of these differences, let us recall that in both 3D and 2D materials, the changes of cation oxidation states are essentially associated with negative values of the corresponding $\Delta_1 = -\Delta_{VBM} + G'$ and are thus likely to take place if Δ_{VBM} is positive and large, $\Delta_{VBM} > G'$. A comparison of the band edge positions in the 2D and 3D parent oxides is given in Fig. 4 and the corresponding values of Δ_1 and Δ_2 are summarized in Tab. 4. Results obtained in hybrid calculations are reported in SI, Fig. S2 and Tab. S4.

While, unsurprisingly, G' is systematically reduced when moving from 3D to 2D, the effect is relatively small (0.2-0.3 eV) in all cases but Cr_2O_3. As a consequence, the difference between 3D and 2D in most cases relies on the changes of Δ_{VBM}. Indeed, its strong decrease

between 3D ($\Delta_{VBM} > 0$) and 2D ($\Delta_{VBM} < 0$) in Ti_2O_3-V_2O_3 suppresses the redox reaction in $TiVO_3$ HC, while its increase in V_2O_3-Fe_2O_3 provokes one in $VFeO_3$ HC. Only for V_2O_3-Cr_2O_3, for which 2D and 3D Δ_{VBM} are similar, the partial redox reaction in the 2D structure is induced by a substantially narrower Cr_2O_3 band gap.

As discussed in Sec. 3, the most pronounced changes of VBM occur in the two Mott-Hubbard oxides (Ti_2O_3 and V_2O_3). They are due to the gap modifications induced by a different crystalline field splitting of the $3d$ multiplet in 3D and 2D structures. It is thus not surprising to find that these two oxides are the constituents of the two mixed compounds ($TiVO_3$ and $VFeO_3$) which show large differences of 3D and 2D characteristics driven by Δ_{VBM}. This picture is consistent with the hybrid results (SI, Fig. S2 and Tab. S4).

Table 5: Formation energies E^{form} of mixed MM'O_3 compounds in their most stable HC (top) or bulk ilmenite[39] (bottom) structures. (eV per formula unit). E^{form} in compounds in which a redox reaction takes place are written in bold type.

	$VFeO_3$	$TiFeO_3$	$TiCrO_3$	$VCrO_3$	$CrFeO_3$	$TiVO_3$
HC	**-0.79**	**-0.70**	-0.23	-0.21	-0.21	0.07
bulk	-0.10	**-0.79**	0.04	0.00	0.08	**-0.35**

As far as formation energies are concerned, Tab. 5 shows that, regardless of the compound dimensionality, the most pronounced tendency for mixing is always associated with the occurrence of a redox reaction. However, while strongly negative E^{form} in 3D compounds are uniquely restricted to cases of such a redox reaction, the formation energies of most mixed 2D compounds are negative, regardless of the presence or absence of changes of cation oxidation state. This is best illustrated by $TiCrO_3$ or $CrFeO_3$ in which, regardless of the dimensionality, the cations maintain their parent-like oxidation state, but which display negative E^{form} and thus a tendency for mixing only in 2D. As a consequence of the enhanced tendency for mixing, most 2D honeycombs favor the A-HC order with a maximum number of mixed MM' cation-cation pairs.

6 Conclusion

Relying on a DFT+U approach, we have studied structural, electronic, and energetic characteristics of a series of pure M_2O_3 and mixed MM'O_3 compounds (M, M' = Ti, V, Cr, and Fe) in (unsupported) 2D honeycomb structures. We find that the HC monolayers of pure oxides display the same Mott-Hubbard (Ti_2O_3 and V_2O_3) or mixed Mott-Hubbard/charge-transfer (Cr_2O_3 and Fe_2O_3) character as their bulk corundum counterparts. However, the electronic structure of the Mott-Hubbard oxides is soundly modified by changes of the crystal field splitting and by the more atomic-like character of the out-of plane components of the d multiplet.

As far as mixed compounds are concerned, we find that, regardless of the precise cationic order (alternating or row-wise structures), the local structural and electronic characteristics of $TiVO_3$, $TiCrO_3$ and $CrFeO_3$ are very close to those of their parent pure oxide monolayers. Conversely, the structural, electronic and magnetic characteristics of $TiFeO_3$, $VFeO_3$, and to some extent also $VCrO_3$ differ substantially from those of their parents due to a change of the cation oxidation states. We show that the occurrence of such reduction-oxidation reactions in these cases is fully consistent with the band offsets between the corresponding parents. Interestingly, the purely d character of the gap edges in the Mott-Hubbard oxides makes their electronic structure particularly sensitive to the cation local environment and thus to the lattice dimensionality, and is responsible for different redox states of the same mixed compound in the three- and two-dimensional structures.

The formation energies of all mixed HC compounds but $TiVO_3$ are negative, thus showing a clear tendency for mixing already at low temperatures. This behavior substantially differs from that in their 3D counterparts, where mixing is mostly favored in the presence of a redox reaction only.

Our findings show that low dimensionality enables stabilization of ternary oxides of compositions and properties with no bulk equivalents, thus of a direct interest for modern technologies. Extension of this work to supported HC structures is in progress.

7 Acknowledgement

We acknowledge fruitful discussions with M. R. Castell, S. Surnev and F. P. Netzer.

8 Supporting Information Available

The Supporting Information contains numerical results of hybrid HSE03 calculations performed on:

- parent M_2O_3 oxides in both unsupported honeycomb and bulk corundum structures: electronic and magnetic properties (Tab. S1); LDOS (Fig. S1); comparison between HC and bulk band edges (Fig. S2)
- mixed MM'O_3 oxides in both unsupported A-HC honeycomb and bulk ilmenite structures: electronic and magnetic properties of A-HC (Tab. S2); comparison between DFT+U and HSE03 LDOS of A-HC (Figs. S3-S4); electronic and magnetic properties of bulk ilmenite MM'O_3 (Tab. S3)
- band alignment between parent HC and bulk oxides (Tab. S4)

This material is available free of charge via the Internet at http://pubs.acs.org.

References

(1) Netzer, F. P.; Fortunelli, A.; Eds., *Oxide materials at the two-dimensional limit*; Springer Series in Materials Science; Springer International Publishing: Cham, Switzerland, 2016; Vol. 234.

(2) Goniakowski, J.; Noguera, C.; Giordano, L. Using polarity for engineering oxide nanostructures: structural phase diagram in free and supported MgO(111) ultrathin films. *Phys. Rev. Lett* **2004**, *94*, 215702.

(3) Claeyssens, F.; Freeman, C. L.; Allan, N. L.; Sun, Y.; Ashfold, M. N.; Harding, J. H. Growth of ZnO thin films–experiment and theory. *J. Mater. Chem.* **2005**, *15*, 139–148.

(4) Tusche, C.; Kirschner, H. L. M. J. Observation of depolarized ZnO(0001) monolayers: formation of unreconstructed planar sheets. *Phys. Rev. Lett.* **2007**, *99*, 026102.

(5) Wu, W.; Lu, P.; Zhang, Z.; Guo, W. Electronic and magnetic properties and structural stability of BeO sheet and nanoribbons. *ACS Appl. Mater. Interfaces* **2011**, *3*, 4787–4795.

(6) Ritter, M.; Ranke, W.; Weiss, W. Growth and structure of ultrathin FeO films on Pt(111)studied by STM and LEED. *Phys. Rev. B* **1998**, *57*, 7240–7251.

(7) Ranke, W.; Ritter, M.; Weiss, W. Crystal structures and growth mechanism for ultrathin films of ionic compound materials: FeO(111) on Pt(111). *Phys. Rev. B* **1999**, *60*, 1527–1530.

(8) Gubo, M.; Ebensperger, C.; Meyer, W.; Hammer, L.; Heinz, K. Sub-stoichiometric cobalt oxide monolayer on Ir(100)-(1×1). *J. Phys.: Condens. Matter* **2009**, *21*, 474211.

(9) Ebensperger, C.; Gubo, M.; Meyer, W.; Hammer, L.; Heinz, K. Substrate-induced structural modulation of a CoO(111) bilayer on Ir(100). *Phys. Rev. B* **2010**, *81*, 235405.

(10) Barcaro, G.; Agnoli, S.; Sedona, F.; Rizzi, G. A.; Fortunelli, A.; Granozzi, G. Structure of reduced ultrathin TiOx polar films on Pt(111). *J. Phys. Chem. C* **2009**, *113*, 5721–5729.

(11) Wu, Q.-H.; Fortunelli, A.; Granozzi, G. Preparation, characterization and structure of Ti and Al ultrathin oxide films on metals. *Int. Rev. Phys. Chem.* **2009**, *28*, 517–576.

(12) Wu, C.; Marshall, M. S. J.; Castell, M. R. Surface structures of ultrathin TiO_x films on Au(111). *J. Phys. Chem. C* **2011**, *115*, 8643–8652.

(13) Wu, C.; Castell, M. R.; Goniakowski, J.; Noguera, C. Stoichiometry engineering of ternary oxide ultrathin films: $Ba_xTi_2O_3$ on Au(111). *Phys. Rev. B* **2015**, *91*, 155424.

(14) Guimond, S.; Haija, M. A.; Kaya, S.; Lu, J.; Weissenrieder, J.; Shaikhutdinov, S.; Kuhlenbeck, H.; Freund, H.-J.; Dobler, J.; Sauer, J. Vanadium oxide surfaces and supported vanadium oxide nanoparticles. *Top. Catal.* **2006**, *38*, 117–125.

(15) Feiten, F. E.; Seifert, J.; Paier, J.; Kuhlenbeck, H.; Winter, H.; Sauer, J.; Freund, H.-J. Surface structure of $V_2O_3(0001)$ revisited. *Phys. Rev. Lett.* **2015**, *114*, 216101.

(16) Möller, C.; Fedderwitz, H.; Noguera, C.; Goniakowski, J.; Nilius, N. Temperature-dependent phase evolution of copper-oxide thin-films on Au(111). *Phys. Chem. Chem. Phys.* **2018**, *20*, 5636–5643.

(17) Köksal, O.; Baidya, S.; Pentcheva, R. Confinement-driven electronic and topological phases in corundum-derived 3*d*-oxide honeycomb lattices. *Phys. Rev. B* **2018**, *97*, 035126.

(18) Goniakowski, J.; Noguera, C. Polarization and rumpling in oxide monolayers deposited on metallic substrates. *Phys. Rev. B* **2009**, *79*, 155433.

(19) Goniakowski, J.; Noguera, C.; Giordano, L.; Pacchioni, G. Adsorption of metal adatoms on FeO(111) and MgO(111) monolayers: Effects of charge state of adsorbate on rumpling of supported oxide film. *Phys. Rev. B* **2009**, *80*, 125403.

(20) Jaffe, J. E.; Bachorz, R. A.; Gutowski, M. Band offset and magnetic property engineering for epitaxial interfaces: A monolayer of M_2O_3 ($M = \mathrm{Al, Ga, Sc, Ti, Ni}$) at the $\alpha{-}Fe_2O_3/\alpha{-}Cr_2O_3$ (0001) interface. *Phys. Rev. B* **2007**, *75*, 205323.

(21) Freund, H.-J.; Pacchioni, G. Oxide ultra-thin films on metals: new materials for the design of supported metal catalysts. *Chem. Soc. Rev.* **2009**, *37*, 2224–2242.

(22) Nilius, N. Properties of oxide thin films and their adsorption behavior studied by scanning tunneling microscopy and conductance spectroscopy. *Surf. Sci. Rep.* **2009**, *64*, 595–659.

(23) Pacchioni, G.; Freund, H.-J. Electron transfer at oxide Surfaces. The MgO paradigm: from defects to ultrathin films. *Chem. Rev.* **2012**, *113*, 4035–4072.

(24) Surnev, S.; Fortunelli, A.; Netzer, F. P. Structure-property relationship and chemical aspects of oxide-metal hybrid nanostructures. *Chem. Rev.* **2012**, *113*, 4314–4372.

(25) Sun, Y.-N.; Giordano, L.; Goniakowski, J.; Lewandowski, M.; Qin, Z.-H.; Noguera, C.; Shaikhutdinov, S.; Pacchioni, G.; Freund, H.-J. The interplay between structure and CO oxidation catalysis on metal- supported ultrathin oxide films. *Angew. Chem. Int. Ed.* **2010**, *49*, 4418.

(26) Giordano, L.; Goniakowski, J.; Pacchioni, G. Properties of MgO(100) ultrathin layers on Pd(100): Influence of the metal support. *Phys. Rev. B* **2003**, *67*, 045410.

(27) Prada, S.; Giordano, L.; Pacchioni, G.; Goniakowski, J. Theoretical description of metal/oxide interfacial properties: The case of MgO/Ag(001). *Appl. Surf. Sci.* **2016**, *390*, 578–582.

(28) Goniakowski, J.; Noguera, C.; Giordano, L. Prediction of uncompensated polarity in ultrathin films. *Phys. Rev. Lett* **2007**, *98*, 205701.

(29) Goniakowski, J.; Giordano, L.; Noguera, C. Polarity compensation in low-dimensional oxide nanostructures: the case of metal-supported MgO nanoribbons. *Phys. Rev. B* **2013**, *87*, 035405.

(30) Barth, T. F. W.; Posnjak, E. The crystal structure of ilmenite. *Zeitschrift Kristallographie* **1934**, *88*, 265–270.

(31) Kramer, A.; Sutter, E.; Su, D.; Batzill, M. Epitaxial corundum-$VTiO_3$ thin films grown on c-cut sapphire. *Thin Solid Films* **2017**, *631*, 85–92.

(32) Mashiko, H.; Oshima, T.; Ohtomo, A. Band-gap narrowing in α-$(Cr_xFe_{1-x})_2O_3$ solid-solution films. *Appl. Phys. Lett.* **2011**, *99*.

(33) Wilson, N. C.; Muscat, J.; Mkhonto, D.; Ngoepe, P. E.; Harrison, N. M. Structure and properties of ilmenite from first principles. *Phys. Rev. B* **2005**, *71*, 075202.

(34) Moore, E. A. First-principles study of the mixed oxide $\alpha-FeCrO_3$. *Phys. Rev. B* **2007**, *76*, 195107.

(35) Benny, S.; Grau-Crespo, R.; de Leeuw, N. H. A theoretical investigation of α-Fe_2O_3-Cr_2O_3 solid solutions. *Phys. Chem. Chem. Phys.* **2009**, *11*, 808–815.

(36) Sadat Nabi, H.; Pentcheva, R. Energetic stability and magnetic coupling in $(Cr_{1-x}Fe_x)_2O_3$: Evidence for a ferrimagnetic ilmenite-type superlattice from first principles. *Phys. Rev. B* **2011**, *83*, 214424.

(37) Yang, H.; Mi, W.; Bai, H.; Cheng, Y. Electronic and optical properties of new multifunctional materials via half-substituted hematite: first principles calculations. *RSC Adv.* **2012**, *2*, 10708–10716.

(38) Pomp, S.; Kuhness, D.; Barcaro, G.; Sementa, L.; Mankad, V.; Fortunelli, A.; Sterrer, M.; Netzer, F. P.; Surnev, S. Two-dimensional iron tungstate: A ternary oxide layer with honeycomb geometry. *J. Phys. Chem. C* **2016**, *120*, 7629–7638.

(39) Le, H.-L. T.; Goniakowski, J.; Noguera, C. Properties of mixed transition metal oxides: MM'O_3 in corundum-type structures (M, M' = Al, Ti, V, Cr, and Fe). *Phys. Rev. Mat.* **2018**, *2*, 085001.

(40) Le, H.-L.; Goniakowski, J.; Noguera, C. (0001) Interfaces between M_2O_3 corundum oxides (M = Al, Ti, V, Cr, Fe). *Surf. Sci.* **2018**, *679*, 17–23.

(41) Kresse, G.; Furthmuller, J. Efficient iterative schemes for ab initio total energy calculations using a plane-wave basis set. *Phys. Rev. B* **1996**, *54*, 11169–11186.

(42) Kresse, G.; Hafner, J. Ab initio molecular dynamics for liquid metals. *Phys. Rev. B* **1993**, *47*, 558–561.

(43) Blöchl, P. E. Projector augmented-wave method. *Phys. Rev. B* **1994**, *50*, 17953–17979.

(44) Kresse, G.; Joubert, D. From ultrasoft pseudopotentials to the projector augmented-wave method. *Phys. Rev. B* **1999**, *59*, 1758–1775.

(45) Dion, M.; Rydberg, H.; Schroder, E.; Langreth, D. C.; Lundqvist, B. I. Van der Waals density functional for general geometries. *Phys. Rev. Lett.* **2004**, *92*, 246401.

(46) Klimes, J.; Bowler, D. R.; Michaelides, A. Chemical accuracy for the van der Waals density functional. *J. Phys.: Cond. Matt.* **2010**, *22*, 022201.

(47) Klimes, J.; Bowler, D. R.; Michaelides, A. Van der Waals density functionals applied to solids. *Phys. Rev. B* **2011**, *83*, 195131.

(48) Anisimov, V. I.; Aryasetiawan, F.; Liechtenstein, A. I. First-principles calculations of the electronic structure and spectra of strongly correlated systems: the LDA+U method. *J. Phys.: Condens. Matter* **1997**, *9*, 767–808.

(49) Dudarev, S. L.; Botton, G. A.; Savrasov, S. Y.; Humphreys, C. J.; Sutton, A. P. Electron-energy-loss spectra and the structural stability of nickel oxide: An LSDA+U study. *Phys. Rev. B* **1998**, *57*, 1505–1509.

(50) Heyd, J.; Scuseria, G.; Ernzerhof, M. Hybrid functionals based on a screened Coulomb potential. *J. Chem. Phys* **2003**, *118*, 8207–8215.

(51) Heyd, J.; Scuseria, G.; Ernzerhof, M. Erratum: "Hybrid functionals based on a screened Coulomb potential" [J. Chem. Phys. 118, 8207 (2003)]. *J. Chem. Phys* **2006**, *124*, 219906–219906.

(52) Bader, R. F. W. A quantum theory of molecular structure and its applications. *Chem. Rev.* **1991**, *91*, 893–928.

(53) Henkelman, G.; Arnaldsson, A.; Jonsson, H. A fast and robust algorithm for Bader decomposition of charge density. *Comput. Mater. Sci.* **2006**, *36*, 354–360.

(54) Momma, K.; Izumi, F. VESTA 3 for three-dimensional visualization of crystal, volumetric and morphology data. *J. Appl. Crystallogr.* **2011**, *41*, 1272–1276.

(55) Monkhorst, H.; Pack, J. Special points for Brillouin-zone integrations. *Phys. Rev. B* **1976**, *13*, 5188–5192.

(56) Shannon, R. D. Revised effective ionic radii and systematic studies of interatomic distances in halides and chalcogenides. *Acta Crystallogr. A* **1976**, *32*, 751–767.

(57) Noguera, C. *Physics and chemistry at oxide surfaces*; Cambridge University Press: Cambridge, New York, Melbourne, Madrid, Cape Town, Singapore, Sao Paulo, Delhi, Tokyo, Mexico City, 2005.

(58) Noguera, C.; Pojani, A.; Casek, P.; Finocchi, F. Electron redistribution in low-dimensional oxide structures. *Surf. Sci.* **2002**, *507–510*, 245–255.

(59) Harrison, W. A. *Electronic structure and the properties of solids*; Freeman: San Francisco, 1980.

(60) Anderson, R. L. Experiments on Ge-GaAs heterojunctions. *Solid-State Electron.* **1962**, *5*, 341–351.

(61) Frensley, W. R.; Kroemer, H. Theory of the energy-band lineup at an abrupt semiconductor heterojunction. *Phys. Rev. B* **1977**, *16*, 2642–2652.

(62) de Walle, C. G. V.; Martin, R. M. Theoretical study of band offsets at semiconductor interfaces. *Phys. Rev. B* **1987**, *35*, 8154–8165.

(63) Massidda, S.; Min, B. I.; Freeman, A. J. Interface phenomena at semiconductor heterojunctions: Local-density valence-band offset in GaAs/AlAs. *Phys. Rev. B* **1987**, *35*, 9871–9874.

(64) Tejedor, C.; Flores, F. A simple approach to heterojunctions. *J. Phys. C* **1978**, *11*, L19–L23.

(65) Flores, F.; Tejedor, C. Energy barriers and interface states at heterojunctions. *J. Phys. C* **1979**, *12*, 731–749.

(66) Tersoff, J. Theory of semiconductor heterojunctions: The role of quantum dipoles. *Phys. Rev. B* **1984**, *30*, 4874–4877.

(67) Zhong, Z.; Hansmann, P. Band alignment and charge transfer in complex oxide interfaces. *Phys. Rev. X* **2017**, *7*, 011023.

Graphical TOC Entry